Solid State Sciences 39 (2015) 69–73

Contents lists available at ScienceDirect

Solid State Sciences

journal homepage: www.elsevier.com/locate/ssscie

Structure and magnetic properties of manganese–zinc-ferrites prepared by spray pyrolysis method

Dzmitry Kotsikau [a, *], Maria Ivanovskaya [b], Vladimir Pankov [a], Yulia Fedotova [c]

[a] Belarusian State University, 14 Leningradskaya, 220030 Minsk, Belarus
[b] Research Institute for Physical-Chemical Problems of the Belarusian State University, 14 Leningradskaya, 220030 Minsk, Belarus
[c] National Centre of Physics of Particles and High Energies, 18 Pervomajskaya str, 220088 Minsk, Belarus

ARTICLE INFO

Article history:
Received 19 June 2014
Received in revised form
7 November 2014
Accepted 26 November 2014
Available online 26 November 2014

Keywords:
Mn–Zn-ferrite
Spray pyrolysis
Structural characterization
Magnetic properties
Mössbauer spectroscopy

ABSTRACT

A spray pyrolysis of a water solution of iron, manganese and iron nitrates is applied to prepare $Zn_{0.5}Mn_{0.5}Fe_2O_4$ single-phase ferrite with a spinel-type structure. The samples are characterized by means of differential scanning calorimetry, scanning and transmission electron microscopy, X-ray diffraction, infrared and ^{57}Fe Mössbauer spectroscopy. The mass magnetization σ and the magnetic susceptibility $1/\chi$ of the ferrites are measured as a function of temperature over the range of 78–728 K. The obtained sample contains nanoparticles with an average diameter d ~7 nm possessing Mn_xZn_y-$Fe_{3-(x+y)}O_4$ spinel-type structure with a uniform distribution of manganese and zinc atoms over the ferrite lattice. The Curie temperature is determined to be 375 ÷ 380 K.

1. Introduction

Nanocrystalline ferrites are still the subject of tremendous interest due to their attractive fundamental electronic and magnetic properties as well as due their potential applications in electronics, microwave and computer technologies [1–19].

The advantageous feature of the spinel-type ferrites is that their properties could be easily tuned and controlled since they depend regularly on the variation of the compositions and the cation distribution in a material. The grain size distribution is also an important parameter affecting the functional characteristics of ferrites [1,8,12,14–16,20].

The studied ferrites can be considered as $Mn_{1-x}Zn_xFe_2O_4$ solid solutions, which differ in a structural and a concentration inhomogeneities. To achieve the best magnetic characteristics, the preparation of a product consisting of a single spinel-type phase with no traces of iron oxide or other ferrite phases like $MnFe_2O_4$ or $ZnFe_2O_4$ is required. The oxidation state of zinc, manganese and iron cations, and the positions they occupy in the spinel crystal lattice also influence the magnetic behavior of the Mn–Zn-ferrites. According to the Neel theory, a maximum magnetization value is reached when bivalent cations (Zn^{2+}, Mn^{2+}) occupy the tetrahedral positions of the spinel lattice, and trivalent cations (Fe^{3+}) are distributed over the octahedral sites [8,21].

In the technological cycle of the ferrite fabrication, $Mn^{2+} \rightarrow Mn^{3+}$ oxidation reaction might occur at high temperatures, which is likely accompanying by a reduction of Fe^{3+} ions to Fe^{2+} state and by a redistribution of the metal cations between the sublattices. Thus, a partial swap of the generated Fe^{2+} and Mn^{3+} ions between the tetrahedral and the octahedral lattice sites is possible. The described processes have an adverse effect on the magnetic features of the material. The oxidation of Mn^{2+} ions is known to proceed most rapidly at 900–1000 °C, while the optimal temperature to produce the Mn–Zn-ferrites lies over the temperature range of 1000–1200 °C. Specific cooling modes, including oxygen control in the furnace chamber, are typically applied to avoid Mn^{2+} oxidation and to produce ferrites with the proper functional features [17]. However, the only reliable way to prepare the ferrites in a form of powder and prevent Mn^{2+} oxidation is to reduce the synthesis temperature. Along with the conventional

Abbreviations: DSC, differential scanning calorimetry; DTG, differential thermal gravimetric analysis; IR, infrared; JCPDS PDF, joint committee on the powder diffraction spectra – powder diffraction file; RT, room temperature; SEM, scanning electron microscopy; TEM, transmission electron microscopy; TG, thermal gravimetric analysis; XRD, X-ray diffraction.

* Corresponding author.
E-mail addresses: kotsikau@bsu.by (D. Kotsikau), ivanovskaya@bsu.by (M. Ivanovskaya), julia@hep.by (Y. Fedotova).

http://dx.doi.org/10.1016/j.solidstatesciences.2014.11.013
1293-2558/

ceramic processing techniques [1,15] a number of modifications of the nanotechnology can be used to obtain nanocrystalline ferrites at comparatively low temperature, in particular, hydrothermal method [1,6,9,12], thermally stimulated dehydration of co-precipitated hydroxides of the corresponding metals [2–5,14,16] and spray pyrolysis of water solutions of metal nitrates [12,18,21–27].

As shown in [18], the spray pyrolysis method based on inorganic metal precursors allows preparing ferrites at temperature below 650 °C. An important point is that this technique provides highly homogeneous distribution of the components in the resulting product since the formation of its structure proceeds within microscopic droplets of the reacting mixture. The size of the resulting particles might be adjusted over a wide range (from 50 nm to 500 mkm) [100]. Non-agglomerated particles with a size down to 10 nm are achieved by applying soluble inert additives to the reaction mixture (NaCl, H_3BO_3 et al.). Furthermore, the inert components allow subsequent thermal treating the generated powder without a noticeable growth in the size [18].

The solution aerosol techniques take advantage of many of the available methods that have been developed for powder synthesis but then uniquely control the particle formation environment by compartmentalizing the solution into droplets. In this manner, the spray pyrolysis ensures a complete stoichiometry retention on the droplet scale, at least, and, thus, is particularly advantageous for mixed metal oxide synthesis. By controlling the type of a thermolysis reaction, a nature of the precursors (organic or inorganic salts, organic compounds, sols of oxides with preset morphology and phase composition), and a nature of a gaseous carrier, it is possible to synthesize oxide, non-oxide ceramic, metal [23], and complex composite particles [18,24]

The spray pyrolysis processes offer a number of opportunities for the synthesis of either hollow or porous particles that may be useful for thermal insulation or catalyst support applications [25]. Analogous to fiber formation by dry spinning, it has been demonstrated that concentration-discontinuous fibers can be produced by this method when using a two-fluid atomizer [26]. The pyrolysis is also well suited for producing thin films of the desired stoichiometry on large, non-planar surfaces [27]. A potential high production rate is another advantage of the chosen synthetic approach [24].

In this paper, we report a study of the structural features and the magnetic properties of Mn–Zn-ferrites prepared using a low-temperature spray pyrolysis of metal nitrates.

2. Materials and methods

A water solution of Zn (II), Mn (II) and Fe (III) nitrates taken in the stoichiometric proportion with a concentration corresponding to 0.25 mol/dm^3 of $Zn_{0.5}Mn_{0.5}Fe_2O_4$ is used to synthesize the Mn–Zn-ferrite by the spray pyrolysis approach. The solution is transformed into an aerosol state with an ultrasonic atomizer and carried in the reaction zone with air or nitrogen (flow rate is 5 l/min). The reaction zone (a quartz tube with l = 1.2 m and d = 42 mm) is situated in a furnace heated to 650 °C. The produced powder are collected in an electrostatic precipitator heated to 200 °C to prevent the condensation of water vapors.

Thermal analysis (DSC, TG, DTG) of the mixed aqueous solution of Zn (II), Mn (II) and Fe (III) nitrates is carried out on a NETZSCH STA 449C instrument using an alumina crucible over temperature range of 30–1000 °C. The sample weight is 54.280 mg.

IR spectra are collected on a Thermo Nicolet AVATAR FTIR-330 spectrometer supplied with a diffuse reflectance accessory over λ range of 400–4000 cm^{-1}.

X-ray diffraction patterns are recorded from the powders on a DRON-2.0 diffractometer with a Ni-filtered CoK_α radiation (λ = 0.178896 nm) over 2θ range of 20–80°. The evaluation of the results and the identification of the ferrite structure are carried out by a standard procedure using JCPDS PDF data.

The morphology of the samples including the estimation of their grain size is analyzed by scanning electron microscopy (SEM) on a LEO 1402 instrument, and by transmission electron microscopy (TEM) on a LEO 903 microscope. In the TEM studies, direct carbon replicas of the surface are examined. The replicas are formed by the deposition of a thin layer of carbon onto the powder samples in a vacuum evaporator. Then the replicas are removed by dissolving the ferrite powder in HCl solution. The etching length that enables to keep some ferrite powder on the carbon films is selected. Then the replicas are picked up onto TEM grids.

Room temperature (RT) ^{57}Fe Mössbauer spectroscopy is applied to reveal the local structure and the magnetic state of the ferrite samples. The spectra are recorded on a MSMS2000 spectrometer in a transmission geometry using a ^{57}Co/Rh source (40 mCi). The spectra are fitted using MOSMOD program assuming the distribution of the hyperfine magnetic field (H_{hf}) and the electric quadrupole splitting (ΔE_Q). All the isomer shifts (δ) are referenced to α-Fe foil.

The mass magnetization σ and the magnetic susceptibility χ of the samples are measured as a function of temperature by Faraday's method in cooling and heating modes with an external magnetic field B = 0.86 T over the range of 78–728 K.

3. Results and discussion

The results of the thermal analysis of the aqueous solution of Zn(II), Mn(II) and Fe(III) nitrates with the metal ratio corresponding to $Zn_{0.5}Mn_{0.5}Fe_2O_4$ composition are shown in Fig. 1. As expected, the nitrates of the given metals melt down at 40–80 °C. Note, that at the earlier stages of the heating, the formation of a colloidal solution may occur owing to the polycondensation of nitrate aquacomplexes via OH-bridges. As a result, mixed polymerized precursors with a general formula [(Fe^{2+}, Mn^{2+}, Zn^{2+}) (NO_x, OH, H_2O)] are formed. Their thermal treatment enables the preparation of a highly homogeneous oxide product. As follows from the results of the thermal analysis, the removal of water and nitrate ions and the formation of metal oxide phases proceed simultaneously below 200 °C. No evidences of a possible Mn^{2+} oxidation are present in the DSC–TG–DTG curves over the temperature range of 200–1000 °C. According to the IR spectroscopy results reported in

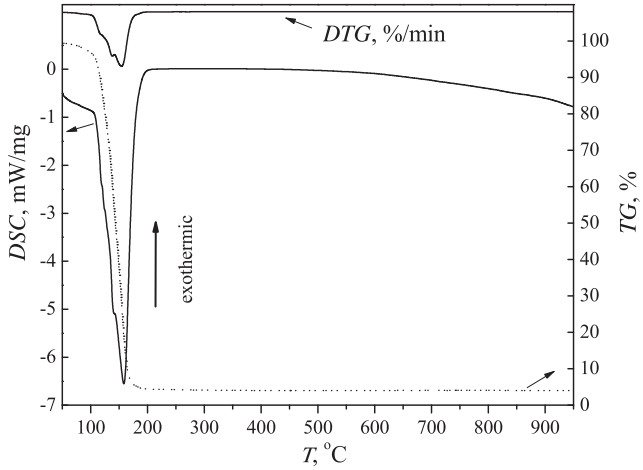

Fig. 1. The DSC, TG and DTG curves recorded from the mixed aqueous solution of Zn(II), Mn(II) and Fe(III) nitrates with Zn:Mn:Fe = 0.5:0.5:2 molar ratio.

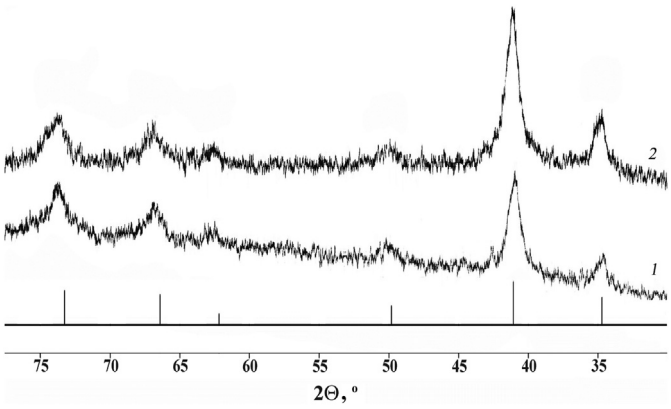

Fig. 2. The XRD patterns of the $Zn_{0.5}Mn_{0.5}Fe_2O_4$ samples prepared in air (1) and in nitrogen (2), and the reference stroke pattern of the spinel lattice.

[28], the removal of NO_x^- anion-radicals occurs most rapidly at 200–300 °C under thermal decomposition of a powder mixture of metal nitrates with the same composition as used in this paper.

The reflections of a spinel-type Mn–Zn–Fe_2O_4 ferrite phase are detected in the X-ray diffraction patterns of the samples synthesized both in air and in nitrogen (Fig. 2). The observed reflections can be attributed to both $Mn_{0.4}Zn_{0.6}Fe_2O_4$ (JCPDS no. 74-2400) and $Mn_{0.6}Zn_{0.4}Fe_2O_4$ (JCPDS no. 74-2401) phases, which have close lattice parameters. The presence of additional phases is not revealed. The broadening of the XRD reflections allows estimating the areas of coherent scattering D^{coh} in the powders that often correspondents to their average grain size. For the studied samples, the values of D^{coh} range between 2 and 7 nm. Note that the broadness of the diffraction reflections did not allow evaluating the precise value of the lattice parameter.

According to the SEM results shown in Fig. 3a, the prepared samples consist of regularly shaped, spherical particles. The surface morphology of the spheres is typical of amorphous or glassy materials. The particle diameters range between 150 nm and 1.6 mkm with a distribution maximum corresponding to 650–800 nm. The samples prepared by spray pyrolysis in nitrogen atmosphere show narrower particle size distribution as compared to the samples synthesized in air. The observed spheres of micrometer size are loose and polycrystalline, and consist of smaller ferrite particles (4–12 nm), which is typical of the samples obtained by the spray pyrolysis processing. Such a fine structure of spheres is clearly seen on the TEM images of the direct carbon replicas of the powder ferrite samples (Fig. 3b). It is noteworthy that the diameter of these

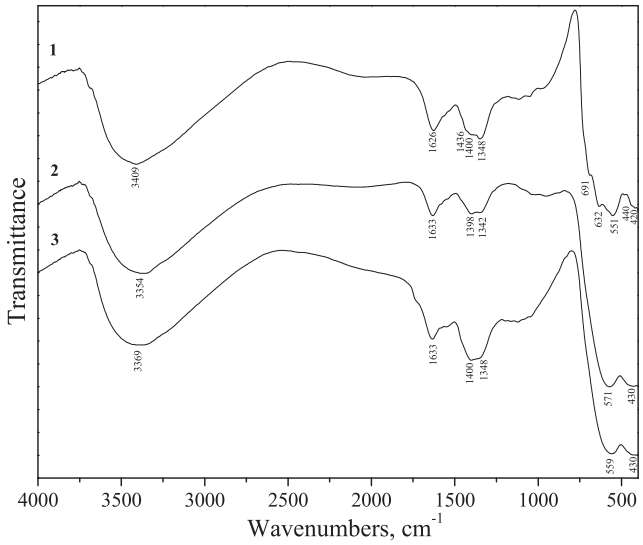

Fig. 4. The IR spectra of γ-Fe_2O_3 (1) and the Mn–Zn-ferrite obtained in nitrogen (2) and in air (3).

particles matches closely the average crystallite size determined by the XRD (D^{coh}).

It is known [29] that the ν_{Fe-O} stretching vibrations and the δ_{Fe-O-H} bending vibrations in iron oxides are strongly influenced by the symmetry of the oxygen coordination and by the force constant of Fe–O bonds. In particular, the ν_{Fe-O} absorption bands in the IR spectra of the spinel-type γ-Fe_2O_3 oxide, obtained by annealing of γ-FeOOH at 300 °C, are centered at 420, 440, 551, 632 and 691 cm^{-1} (Fig. 4, spectrum 1).

As reported in [30,31], the formation of zinc or cobalt ferrites by introduction of Zn^{2+} and Co^{2+} ions into γ-Fe_2O_3 is accompanied by a shift of the main ν_{Fe-O} band towards higher frequencies. The similar changes are observed for our samples in Fig. 4 if one compares individual γ-Fe_2O_3 oxide and the Mn–Zn-ferrite samples (420 → 430 cm^{-1}, 551 → 559 (571) cm^{-1}). The absence of an adsorption band assigned to the γ-Fe_2O_3 phase (632, 691 cm^{-1}) in the spectra 2 and 3 confirms the formation of the ferrite structure. A symmetric shape of the ν_{Fe-O} bands in the IR spectra of the ferrites testifies for high homogeneity of the $Mn_{0.5}Zn_{0.5}Fe_2O_4$ spinel structure and the uniformity of Zn^{2+} and Mn^{2+} distribution over the lattice.

IR absorption bands attributed to the bending vibrations of the OH groups directly bonded with metal cations (δ_{M-O-H}) are known

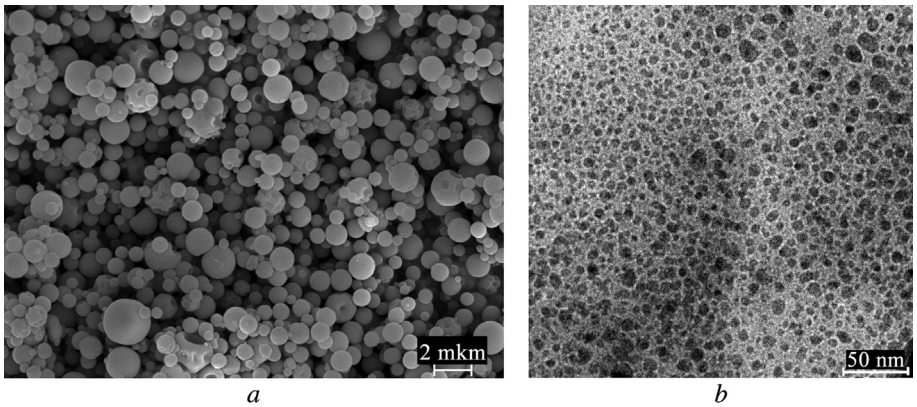

Fig. 3. The SEM (a) and the TEM (b) images of the Mn–Zn-ferrite obtained in nitrogen.

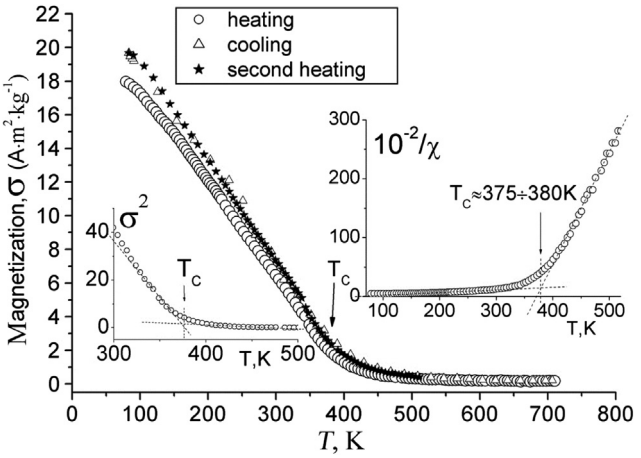

Fig. 5. The temperature dependences of magnetization σ, the squared magnetization σ^2, and the magnetic susceptibility 1/χ measured for the Mn–Zn-ferrite obtained in nitrogen.

Table 1
The parameters of the ^{57}Fe Mössbauer spectra recorded for the Mn–Zn-ferrite samples obtained in air and nitrogen atmosphere.

Synthesis atmosphere	δ, mm/s ±0.03	ΔE_Q, mm/s ±0.03	H_{hf}, T ±0.5	Γ, mm/s ±0.08
Air	0.33	0.53	0	1.14
Nitrogen	0.34	0.42	0	1.02

to be highly sensitive to a degree of structural order in composite oxides [29,32]. Therefore, the region of IR spectra around the mentioned band can be used to evaluate the structural perfection of multicomponent spinel-type oxides. The characteristic bands of the Mn–Zn-ferrites are 832 cm^{-1} (δ_{Zn-O-H}) and 946 cm^{-1} (δ_{Mn-O-H}). The bands around 1030–1122 cm^{-1} attributed to δ_{Fe-O-H} vibrations in the ferrites are also shifted against the corresponding bands of γ-Fe_2O_3 reflecting the effect of Zn^{2+} and Mn^{2+} cations. It can be concluded that the synthesized samples have $Mn_xZn_yFe_{3-(x+y)}O_4$ spinel-type structure with a uniform distribution of manganese and zinc atoms over the ferrite lattice.

The temperature-dependent magnetization $\sigma = f(T)$, the squared magnetization $\sigma^2 = f(T)$ and the magnetic susceptibility $1/\chi = f(T)$ curves for the ferrite sample obtained in nitrogen atmosphere are shown in Fig. 5. The Curie temperature T_C is determined to be 375 ÷ 380 K. These values are consistent with the T_C range theoretically calculated for $Mn_{0.5}Zn_{0.5}Fe_2O_4$ ferrite under variation of Fe^{3+} distribution over the crystal lattice (365 ÷ 385 K). The magnetic measurements do not reveal the formation of individual iron oxide phases, namely γ-Fe_2O_3 (T_C = 865 K) and α-Fe_2O_3 (T_N = 965 K). The shape of the $\sigma = f(T)$ curves and the σ values measured over the temperature range of 100 ÷ 300 K are expected for nanosized ferrites with equal Mn and Zn molar concentrations.

The Mössbauer spectra of the ferrite samples synthesized in nitrogen and in air flow are presented in Fig. 6. The RT spectra represent quadrupole doublets with the parameters indicating a paramagnetic state of Fe^{3+}, while Fe^{2+} state is not revealed. Note that the paramagnetic state is typical of nanosized Mn–Zn-ferrites below their Curie point. Similar parameters of the spectra of the ferrites obtained in nitrogen and in air, listed in Table 1, suggest that $Mn^{2+} \rightarrow Mn^{3+}$ and $Fe^{3+} \rightarrow Fe^{2+}$ reactions do not proceed under the given synthesis conditions. The isomer shift values measured for the samples (δ = 0.33 ÷ 0.34 mm/s) are characteristic of Fe^{3+} ions in oxide solid solutions, including Mn–Zn-ferrites, and indicate a significant ionic contribution into Fe^{3+}–O covalent bonds [32]. The observed broadening of the Mössbauer peaks in Fig. 6 is caused by a combination of a poor crystallinity of the ferrite phase and nanoscaled particles in correlation with the XRD and the TEM results.

The values of ΔE_Q (0.42 ÷ 0.53 mm/s) lie between the values characteristic of individual $MnFe_2O_4$ (0.54 mm/s) and $ZnFe_2O_4$ (0.32 mm/s) ferrites that confirms the formation of the expected $Zn_{0.5}Mn_{0.5}Fe_2O_4$ composition. The quadrupole splitting observed in the Mössbauer spectra is due to a distorted symmetry of the oxygen coordination of Fe^{3+} ions occupying the octahedral sites of the lattice. The distortion arises from the filling of the tetrahedral sites of the spinel lattice by Zn^{2+} and Mn^{2+} ions, which have the diameters greater than for Fe^{3+} ions. A local distortion of the oxygen coordination can also be evoked by Mn^{3+} ions occurred in the ferrite structure. However, this process was not confirmed since a decrease in neither T_C nor σ values were observed for the studied ferrites.

4. Conclusions

A single-phase $Zn_{0.5}Mn_{0.5}Fe_2O_4$ ferrite with a spinel-type structure is prepared by the spray pyrolysis of a water solution of Fe(III), Mn(II) and Fe(III) nitrates at 650 °C. The ferrite sample consists of primary particles with d ~7 nm, which are aggregated into spherical particles with d = 0.15–1.6 mkm. The phase composition, the nanosized state and the high the uniformity of Zn^{2+} and Mn^{2+} distribution over the lattice of the sample is confirmed by RT Mössbauer spectroscopy and magnetic measurements over the temperature range of 78–728 K. The Curie temperature of the $Zn_{0.5}Mn_{0.5}Fe_2O_4$ powder was determined to be 375 ÷ 380 K.

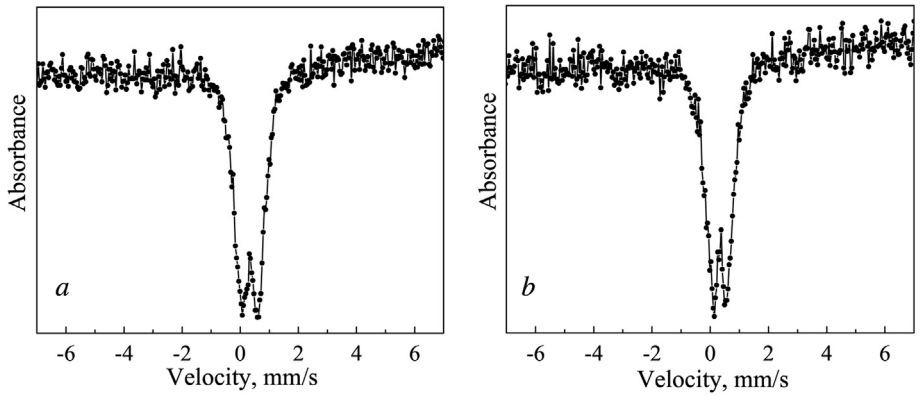

Fig. 6. The ^{57}Fe Mössbauer spectra recorded for the Mn–Zn-ferrite samples obtained in air (a) and nitrogen (b) atmosphere.

References

[1] R.C. Pullar, Hexagonal ferrites: a review of the synthesis, properties and applications of hexaferrite ceramics, Prog. Mater. Sci. 57 (7) (2012) 1191–1334.
[2] Y. Xie, X. Hong, C. Yu, et al., Preparation and magnetic properties of poly (3-octyl-thiophene)/$BaFe_{11.92}(LaNd)_{0.04}O_{19}$-titanium dioxide/multiwalled carbon nanotubes nanocomposites, Comp. Sci. Tech. 77 (2013) 8–13.
[3] Y. Xie, X. Hong, J. Liu, et al., Synthesis and electromagnetic properties of $BaFe_{11.92}(LaNd)_{0.04}O_{19}$/titanium dioxide composites, Mater. Res. Bull. 50 (2014) 483–489.
[4] J. Zhao, Y. Xie, C. Yu, et al., Preparation and characterization of the graphene–carbon nanotube/$CoFe_2O_4$/polyaniline composite with reticular branch structures, Mater. Chem. Phys. 142 (1) (2013) 395–402.
[5] Y. Xie, J. Zhao, Z. Le, et al., Preparation and electromagnetic properties of chitosan-decorated ferrite-filled multi-walled carbon nanotube/polythiophene composites, Comp. Sci. Tech. 99 (2014) 141–146.
[6] J. Zhao, Y. Xie, M. Li, et al., Preparation of magnetic-conductive $Mn_{0.6}Zn_{0.4}Fe_2O_4$-CNTs/PANI nanocomposites through hydrothermal synthesis coupled with in-situ polymerization, Comp. Sci. Tech. 99 (2014) 147–153.
[7] N. Somaiah, T.V. Jayaraman, P.A. Joy, D. Das, Magnetic and magnetoelastic properties of Zn-doped cobalt-ferrites – $CoFe_{2-x}Zn_xO_4$ (x = 0, 0.1, 0.2, and 0.3), J. Magn. Magn. Mater. 324 (14) (2012) 2286–2291.
[8] H. Lin, B. Sun, L. Wang, et al., Development of powder preparation technology and additives in MnZn ferrites, J. Univ. Sci. Tech. Liaoning 4 (2012) 008.
[9] D. Cai, J. Li, T. Tong, et al., Phase evolution of bismuth ferrites in the process of hydrothermal reaction, Mater. Chem. Phys. 134 (1) (2012) 139–144.
[10] V. Duffort, V. Caignaert, V. Pralong, et al., Rich Crystal chemistry and magnetism of "114" stoichiometric $LnBaFe_4O_7$ ferrites, Inorg. Chem. 52 (18) (2013) 10438–10448.
[11] M.A. Gabal, R.M. El-Shishtawy, Y.M. Al Angari, Structural and magnetic properties of nano-crystalline Ni–Zn ferrites synthesized using egg-white precursor, J. Magn. Magn. Mater. 324 (14) (2012) 2258–2264.
[12] M. Sugimoto, The past, present, and future of ferrites, J. Am. Ceram. Soc. 82 (1999) 269–280.
[13] K. Yasuda, Y. Mochizuki, M. Takaya, Multilayer ferrite chip component for growth of microelectronics, in: Proc. of the Eight International Conference of Ferrites, Kyoto, 2000, pp. 1162–1164.
[14] W.C. Kim, S.J. Kim, Y.R. Uhm, C.S. Kim, Magnetic properties of NiZnCu ferrite powders and thin films prepared by a sol-gel method, IEEE Trans. Magn. 37 (2001) 2363–2365.
[15] Z. Pedzich, M. Bucko, M. Krolikowski, M. Bakalarska, J. Babiarz, Microstructure and properties of Mg-Zn ferrite as a result of sintering temperature, J. Eur. Ceram. Soc. 24 (2004) 1053–1056.
[16] C. Corot, P. Robert, J.-M. Idee, M. Port, Recent advances in iron oxide nanocrystal technology for medical imaging, Adv. Drug Deliv. 58 (2006) 1471–1504.
[17] J. Töpfer, A. Angermann, Nanocrystalline magnetite and Mn–Zn ferrite particles via the polyol process: synthesis and magnetic properties, Mater. Chem. Phys. 129 (2011) 337–342.
[18] V. Pankov, Modified aerosol synthesis for nanoscale hexaferrite particles preparation, Mater. Sci. Eng. A 224 (1997) 101–106.
[19] S.S. Khot, N.S. Shinde, B.P. Ladgaonkar, B.B. Kale, S.C. Watawe, Characterization and cytotoxicity of magnetic nanoparticles on breast cancer cells, Adv. Appl. Sci. Res. 2 (4) (2011) 460–471.
[20] St Fisher, C. Michalk, W. Topelmann, Investigation into phase formation of nickel-zink ferrites by hydroxide coprecipitation, Ceram. Int. 18 (5) (1992) 317–320.
[21] K. Kumar, A. Petrovich, C. Williams, Chemically homogeneous fine-grained Mn-Zn ferrites by spray drying, J. Appl. Phys. 65 (5) (1998) 2014–2016.
[22] M.I. Ivanovskaya, A.I. Tolstik, D.A. Kotsikau, V.V. Pankov, The structural characterization of Zn-Mn ferrite synthesized by spray pyrolysis, Russ. J. Phys. Chem. A 83 (12) (2009) 2081–2086.
[23] R.R. Chamberlin, J.S. Skarman, Chemical spray process for inorganic films, J. Electrochem. Soc. 113 (8–9) (1966) 113–119.
[24] G. Messing, S.-C. Zhang, V. Jayanthy, Ceramic powder synthesis by Spray pyrolysis, J. Am. Chem. Soc. 76 (11) (1993) 2707–2726.
[25] R.R. Ciminelli, G.L. Messing, The Chemical and Structural Transformations in the System Aluminum Nitrate/Alumina, vol. 30, Ceramica, Sao Paulo, 1984, pp. 131–138.
[26] A. Ziabicki, Fundamentals of Fiber Formation, Wiley, New York, 1976, p. 488.
[27] G. Blancher, C.R. Fincher Jr., High-temperature deposition of HTSC thin films by spray pyrolysis, Supercord. Sci. Technol. 4 (1991) 69–72.
[28] M. Ivanovskaya, Ceramic and film metaloxide sensors obtained by sol-gel method: structural features and gas-sensitive properties, Electron Tech. 33 (1–2) (2001) 108–112.
[29] K. Nakamoto, Infrared and Raman Spectra of Inorganic and Coordination Compounds, Part B, sixth ed., Wiley, New York, 2009, p. 424.
[30] B. Gillot, F. Jemalli, A. Rousset, Infrared studies on the behaviour in oxygen of cobalt-substituted magnetites: comparison with zinc-substituted magnetites, J. Solid State Chem. 50 (1983) 138–145.
[31] B. Gillot, R.M. Benloucif, A. Rousset, A study of infrared absorption in the oxidation of zinc-substituted magnetites to defect phase γ and hematite, J. Solid State Chem. 39 (1981) 329–336.
[32] J. Sawicki, The Mössbauer study of normal ferrites with the spinel structure, Chechosl. J. Phys. 17 (1967) 371–375.